Inorganic Chemistry
Cite This: Inorg. Chem. XXXX, XXX, XXX−XXX
Article
pubs.acs.org/IC

Electrocatalytic CO_2 Reduction with *Cis* and *Trans* Conformers of a Rigid Dinuclear Rhenium Complex: Comparing the Monometallic and Cooperative Bimetallic Pathways

Weiwei Yang,[†,‡] Sayontani Sinha Roy,[†,‡] Winston C. Pitts,[†] Rebekah L. Nelson,[†] Frank R. Fronczek,[§] and Jonah W. Jurss*[,†]

[†]Department of Chemistry and Biochemistry, University of Mississippi, University, Mississippi 38677, United States
[§]Department of Chemistry, Louisiana State University, Baton Rouge, Louisiana 70803, United States

Supporting Information

ABSTRACT: Anthracene-bridged dinuclear rhenium complexes are reported for electrocatalytic carbon dioxide (CO_2) reduction to carbon monoxide (CO). Related by hindered rotation of each rhenium active site to either side of the anthracene bridge, *cis* and *trans* conformers have been isolated and characterized. Electrochemical studies reveal distinct mechanisms, whereby the *cis* conformer operates via cooperative bimetallic CO_2 activation and conversion and the *trans* conformer reduces CO_2 through well-established single-site and bimolecular pathways analogous to Re(bpy)$(CO)_3$Cl. Higher turnover frequencies are observed for the *cis* conformer (35.3 s^{-1}) relative to the *trans* conformer (22.9 s^{-1}), with both outperforming Re(bpy)$(CO)_3$Cl (11.1 s^{-1}). Notably, at low applied potentials, the *cis* conformer does not catalyze the reductive disproportionation of CO_2 to CO and CO_3^{2-} in contrast to the *trans* conformer and mononuclear catalyst, demonstrating that the orientation of active sites and structure of the dinuclear *cis* complex dictate an alternative catalytic pathway. Further, UV−vis spectroelectrochemical experiments demonstrate that the anthracene bridge prevents intramolecular formation of a deactivated Re−Re-bonded dimer. Indeed, the *cis* conformer also avoids intermolecular Re−Re bond formation.

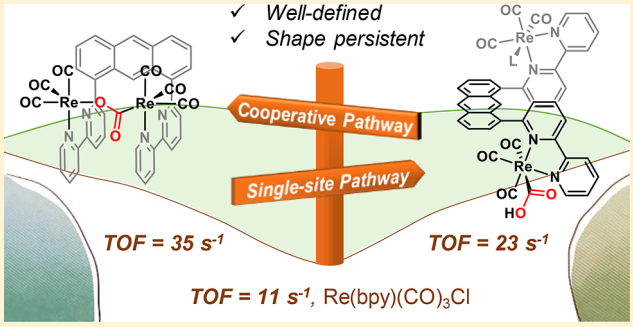

INTRODUCTION

Roughly 85% of the world's energy is derived from burning nonrenewable fossil fuels that generate greenhouse gases.[1] Carbon dioxide (CO_2) is the chief component of this waste stream, which has been linked to climate change and other environmental concerns.[2] Renewable energy sources such as wind and solar are attractive, but they are intermittent, site-specific, and geographically diffuse. Additionally, they require energy storage before they can be relied on to power society.[3] To address this challenge while reducing CO_2 emissions, solar energy or renewable electricity can be used to drive the conversion of CO_2 and water (H_2O) into fuels, whereby energy is stored indefinitely in the form of chemical bonds for on-demand use. The efficient catalytic conversion of CO_2 into energy-rich compounds could close the carbon cycle and allow an underutilized resource to be tapped into.[4]

Molecular metal-based catalysts for CO_2 reduction have been widely pursued, in part because transition metals generally have multiple redox states accessible to facilitate multielectron chemistry. The bulk of these catalysts employ a single metal center.[4] Re(bpy)$(CO)_3$Cl (where bpy is 2,2′-bipyridine) and related derivatives continue to attract attention as competent electrocatalysts for CO_2 reduction, in addition to being single-component photocatalysts.[5−17] Recently, these systems have been functionalized with phosphonate anchoring groups for surface attachment to photocathodes, where they exhibit long-term stability for CO_2 reduction.[18−21] Successful translation of these catalysts into working devices emboldens their continued development, where lower overpotentials and faster rates are remaining challenges.

Mechanistic studies of Re(bpy)$(CO)_3$X-type catalysts have provided evidence for the concentration-dependent formation of dinuclear intermediates during catalysis.[6,7,22−31] Indeed, bimetallic and monometallic pathways exist as dimer formation is in competition with CO_2 reduction at a single metal.[24] Disentangling the contributions of competing pathways, in addition to the transient nature of their respective intermediates, has made it difficult to assess the possible advantages of two metal centers in activating and reducing CO_2 in a cooperative fashion. A beneficial interaction between two active sites is further clouded because a Re−Re-bonded dimer has been indicted as a deactivated intermediate.[27,28]

Several bimetallic catalyst designs have been pursued based on flexible alkyl tethers[32,33] or hydrogen-bonding interactions,[34] which suffer from a lack of rigidity and variable

Received: June 26, 2018

DOI: 10.1021/acs.inorgchem.8b01775
Inorg. Chem. XXXX, XXX, XXX−XXX

solution compositions. Other examples feature dinucleating scaffolds that preclude intramolecular bimetallic CO_2 activation and conversion.[35,36] Thus, the desirable design parameters surrounding this approach are poorly understood. In this context, we sought to develop catalysts with a rigid dinucleating ligand that positions two rhenium active sites in close proximity with a predictable intermetallic distance and orientation (Scheme 1). The ability to isolate and even select

Scheme 1. Synthesis of 1 and Its Bimetallic Rhenium(I) Conformers, *cis*-Re_2Cl_2 and *trans*-Re_2Cl_2

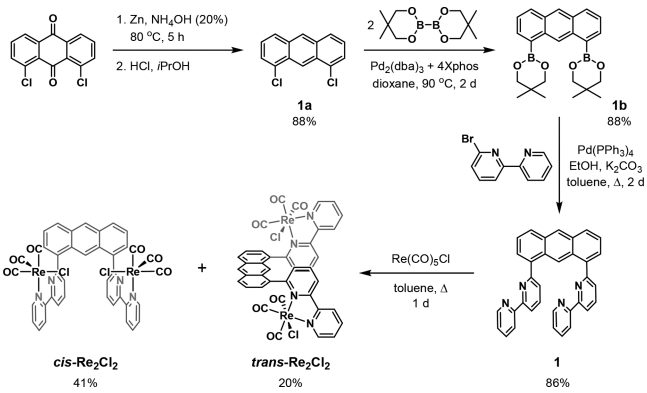

from competing mechanisms (i.e., bimetallic vs monometallic pathways) would allow us to compare and understand differences in efficiency, activity, and stability. Herein, the synthesis, characterization, and electrocatalytic activity of homogeneous *cis* and *trans* conformers of a Re_2 catalyst supported by an anthracene-based polypyridyl ligand are described.

■ SYNTHESIS AND CHARACTERIZATION

The synthesis of 1,8-bis(2,2′-bipyridin-6-yl)anthracene (**1**) and its metalation to generate conformers *cis*-Re_2Cl_2 and *trans*-Re_2Cl_2 is shown in Scheme 1. As previously described,[37] 1,8-dichloroanthraquinone is reduced with zinc to give 1,8-dichloroanthracene (**1a**). Next, the 1,8-diboronate ester (**1b**) is furnished by a palladium-catalyzed borylation with bis(neopentyl glycolato)diboron.[38] The boronate ester is reacted directly by Suzuki cross-coupling with 6-bromo-2,2′-bipyridine to give new dinucleating ligand **1** in 86% yield. Metalation was achieved by refluxing the ligand with 2 equiv of $Re(CO)_5Cl$ in anhydrous toluene overnight to give a mixture of two dinuclear rhenium(I) conformers, *cis*-Re_2Cl_2 and *trans*-Re_2Cl_2. Despite the possible formation of up to seven isomers (Figure S1), only two species are observed in the reaction mixture under these conditions, as shown in the crude ^{1}H NMR spectrum (Figure S2). Two narrow, closely spaced bands were separated by silica gel chromatography to give an overall isolated yield of 61%.[39] We note that solvent-dependent isomer formation was reported previously for di- and trinuclear $Re(CO)_3$-based compounds.[40] ^{1}H NMR spectra of the purified *cis* and *trans* conformers are shown in Figure 1. From the NMR spectra, there is a symmetric species (*cis*-Re_2Cl_2) with 12 chemically distinct protons and an asymmetric species (*trans*-Re_2Cl_2) displaying 22 different proton signals. IR spectroscopy in *N*,*N*-dimethylformamide (DMF) established the presence of *fac*-$Re(CO)_3$ fragments with carbonyl stretching frequencies ν(CO) for *cis*-Re_2Cl_2 at 2019, 1915, and 1890 cm^{-1} and for *trans*-Re_2Cl_2 at 2014, 1910, and 1888 cm^{-1} (Figure S3). For

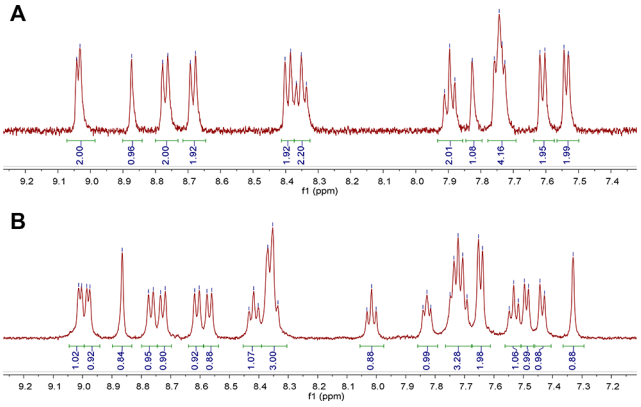

Figure 1. ^{1}H NMR spectra (500 MHz, DMSO-d_6) showing the aromatic region of (A) *cis*-Re_2Cl_2 and (B) *trans*-Re_2Cl_2.

comparison, the CO stretching frequencies of the parent complex, *fac*-Re(bpy)$(CO)_3$Cl, are at 2019, 1914, and 1893 cm^{-1} in DMF.[6]

X-ray-quality crystals of the asymmetric *trans* conformer were obtained by slow isopropyl ether diffusion into a concentrated DMF solution. The crystal structure of *trans*-Re_2Cl_2 is shown in Figure 2, concurrently lending support for a

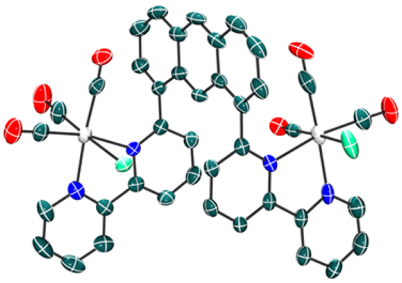

Figure 2. Crystal structure of *trans*-Re_2Cl_2. Hydrogen atoms are omitted for clarity. Thermal ellipsoids are shown at the 70% probability level.

symmetric configuration of the *cis* conformer, which is accessible by rotation (*cis* ↔ *trans*), as observed at elevated temperatures by ^{1}H NMR. However, no interconversion was observed at room temperature over the course of 2 days.

Our catalyst design aims to channel reactivity through a single mechanism by allowing both active sites to be in close proximity for cooperative catalysis or by isolating each metal center for single-site activity. Importantly, because active sites are generated following chloride dissociation from the metal, two symmetric *cis* conformers are possible, one in which the chloro ligands face each other (*cis*-Re_2Cl_2) and another that has its chloro ligands oriented outward (*cis*-**2**, as labeled in Figure S1). Density functional theory (DFT) calculations were used to investigate the barrier to rotation of Re(bpy) moieties to either side of the anthracene bridge by which the *trans* conformer may interconvert to either of the symmetric *cis* conformers in solution. Since the structure of *trans*-Re_2Cl_2 is known, the energy barrier associated with rotational isomerization from *trans*-Re_2Cl_2 was calculated (Figure S5). By DFT, the barrier to rotation from the *trans* conformer to *cis*-Re_2Cl_2 (27.2 kcal mol^{-1}) is 4.6 kcal mol^{-1} lower in energy than the rotation to *cis*-**2** (31.8 kcal mol^{-1}). These calculations provide indirect evidence that the isolated *cis* conformer has its chloro ligands facing "in" (denoted *cis*-Re_2Cl_2, as depicted in Scheme

DOI: 10.1021/acs.inorgchem.8b01775
Inorg. Chem. XXXX, XXX, XXX−XXX

1). Toward more direct evidence, the IR spectra of *cis*-Re_2Cl_2 and *cis*-**2** were calculated by DFT. Notably, *cis*-Re_2Cl_2 is expected to have three ν(CO) absorption bands, while *cis*-**2** is calculated to have four ν(CO) vibrational modes (Figure S4). The experimental Fourier transform infrared (FTIR) spectrum of the *cis* conformer (Figure S3) is in good agreement with the calculated spectrum of *cis*-Re_2Cl_2, further corroborating its specified stereochemistry.

■ ELECTROCHEMISTRY

Following characterization, the redox behaviors of *cis*-Re_2Cl_2 and *trans*-Re_2Cl_2 were analyzed in the absence of CO_2 by cyclic voltammetry in anhydrous DMF containing 0.1 M tetrabutylammonium hexafluorophosphate (Bu_4NPF_6) supporting electrolyte. Re(bpy)$(CO)_3$Cl and a mononuclear derivative (anthryl-Re) bearing a pendant anthracene (shown in Figure 3) were studied in parallel to provide insight into the catalytic

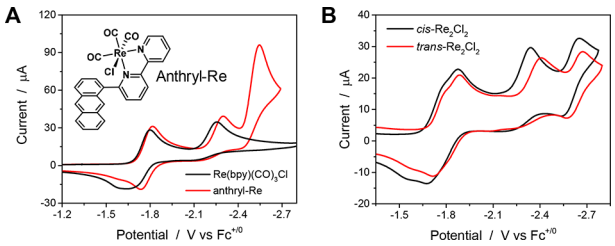

Figure 3. CVs of (A) 2 mM Re(bpy)$(CO)_3$Cl and anthryl-Re and (B) 1 mM *cis*-Re_2Cl_2 and *trans*-Re_2Cl_2 in DMF/0.1 M Bu_4NPF_6 under argon. Glassy carbon disk; ν = 100 mV s^{-1}.

activity and ligand-based redox chemistry. Cyclic voltammograms (CVs) were referenced internally at the end of the experiments to the ferrocenium/ferrocene ($Fc^{+/0}$) couple. The electrochemical properties of Re(bpy)$(CO)_3$Cl have been studied extensively, most often in acetonitrile solutions. Its CV in DMF, overlaid with that of anthryl-Re (Figure 3A), exhibits a quasi-reversible redox process with $E_{p,c}$ at −1.80 V versus $Fc^{+/0}$ and an irreversible reduction at −2.25 V. Notably, the CV of anthryl-Re has a third reduction at −2.54 V that is absent in the parent complex. Similar behavior is observed for the dinuclear catalysts (Figure 3B). The CVs of *cis*-Re_2Cl_2 and *trans*-Re_2Cl_2 reveal two closely spaced, quasi-reversible, one-electron reductions at $E_{p,c}$ = −1.77 and −1.87 V and at −1.78 and −1.88 V, respectively, followed by reductions at $E_{p,c}$ = −2.34 and −2.65 V and at −2.40 and −2.67 V, respectively, with a scan rate of 100 mV s^{-1}. The number of electrons transferred in each redox process based on integrated cathodic peak areas corresponds to a 1:1:2:1 stoichiometry. From scan rate-dependent CVs of the dinuclear conformers and both mononuclear complexes, linear fits were obtained in plots of the reductive peak current ($i_{p,c}$) versus the square root of the scan rate ($\nu^{1/2}$) consistent with freely diffusing systems (Figures S6−S9).[41]

Comproportionation constants (K_C) for the dinuclear catalysts were estimated from the overlapping one-electron reductions as a measure of electronic coupling between Re(bpy) units.[42] Based on the difference in potentials, ΔE, between $E_{p1,c}$ and $E_{p2,c}$, a K_C value of 50 was calculated for both Re_2 conformers, indicative of weak electronic coupling through the anthracene bridge.[42] Weak electronic coupling is not surprising given the number of bonds between redox sites. These results are summarized in Table 1.

Table 1. Reduction Potentials, Diffusion Coefficients, and Comproportionation Constants (K_C) from Cyclic Voltammetry in Anhydrous DMF/0.1 M Bu_4NPF_6 Solutions

catalyst	$E_{p1,c}$	$E_{p2,c}$	$E_{p3,c}$	$E_{p4,c}$
cis-Re_2Cl_2	−1.77	−1.87	−2.34	−2.65
		K_C = 50		
trans-Re_2Cl_2	−1.78	−1.88	−2.40	−2.67
		K_C = 50		
Re(bpy)$(CO)_3$Cl	−1.80	−2.25		
		D = 5.40 × 10^{-6} cm^2 s^{-1}		
anthryl-Re	−1.82	−2.29	−2.54	
		D = 5.48 × 10^{-6} cm^2 s^{-1}		

On the basis of these results and previous work,[34,36,43] we assign the most positive overlapping one-electron redox events to ligand-centered bipyridine reductions to form $[Re^I(bpy^\bullet)(CO)_3Cl]^-$ moieties followed by a third (overall) reductive process that involves overlapping reductions of each of the Re(bpy) units and totals two electrons. The most negative redox event is ascribed to a one-electron, anthracene-based reduction. A CV of free ligand **1** is shown in Figure S10.

Electrocatalytic CO_2 reduction by the dinuclear conformers and monomers Re(bpy)$(CO)_3$Cl and anthryl-Re was then investigated by cyclic voltammetry. The CVs of *cis*-Re_2Cl_2 and *trans*-Re_2Cl_2 at 1 mM concentrations and of monomers at concentrations of 2 mM are shown in Figure 4 in DMF solutions under argon and CO_2 atmospheres. The monomer catalyst concentrations were doubled to maintain a consistent concentration with respect to rhenium.

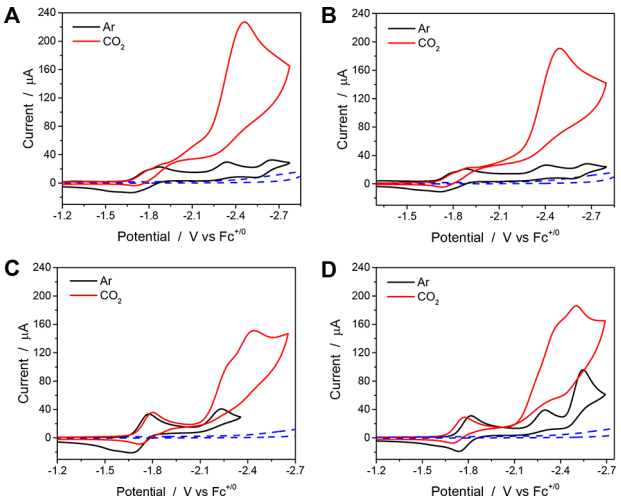

Figure 4. Cyclic voltammetry in argon- and CO_2-saturated DMF/0.1 M Bu_4NPF_6 solutions with (A) 1 mM *cis*-Re_2Cl_2, (B) 1 mM *trans*-Re_2Cl_2, (C) 2 mM Re(bpy)$(CO)_3$Cl, and (D) 2 mM anthryl-Re. Glassy carbon disk; ν = 100 mV s^{-1}. The background under CO_2 is shown with a dashed blue line.

For an electrocatalytic reaction involving heterogeneous electron transfers at the electrode surface, the peak catalytic current is described by eq 1:[44−46]

$$i_{cat} = n_{cat}FA[cat](Dk_{cat}[S]^y)^{1/2} \quad (1)$$

where i_{cat} is the limiting catalytic current in the presence of CO_2, n_{cat} corresponds to the number of electrons transferred in the catalytic process (here n_{cat} = 2 as CO_2 is reduced to CO), F is Faraday's constant, A is the area of the electrode, [cat] is the

DOI: 10.1021/acs.inorgchem.8b01775
Inorg. Chem. XXXX, XXX, XXX−XXX

molar concentration of the catalyst, D is the diffusion coefficient, k_{cat} is the rate constant of the catalytic reaction, and [S] is the molar concentration of dissolved CO_2. By applying eq 1, the catalytic mechanisms of *cis*-Re_2Cl_2 and *trans*-Re_2Cl_2 were probed using cyclic voltammetry to determine the reaction orders with respect to [CO_2] and [cat] (Figures S11 and S12, respectively).

First, gas mixtures of argon and CO_2 were used to vary the partial pressure of CO_2 from 0 to 1 atm to reveal a linear increase in the catalytic current for CO_2 reduction as a function of the square root of dissolved CO_2 concentration for both *cis*-Re_2Cl_2 and *trans*-Re_2Cl_2 catalysts (Figure 5). The concentration of dissolved CO_2 in DMF under saturation conditions at 1 atm is 0.20 M.[47]

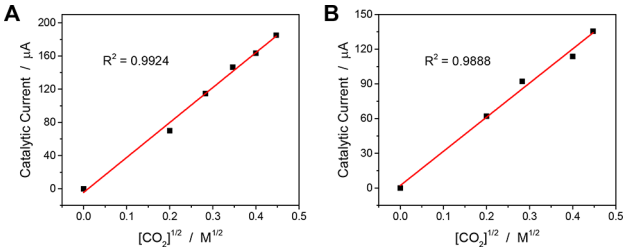

Figure 5. CO_2 concentration dependences for (A) 1 mM *cis*-Re_2Cl_2 and (B) 1 mM *trans*-Re_2Cl_2 in DMF/0.1 M Bu_4NPF_6. Glassy carbon disk; ν = 100 mV s^{-1}. The catalytic current (μA) is plotted versus the square root of [CO_2].

Likewise, the dependence of the catalytic current (i_{cat}) on the concentration of each dinuclear rhenium catalyst ([cat]) in CO_2-saturated solutions was determined (Figure 6).

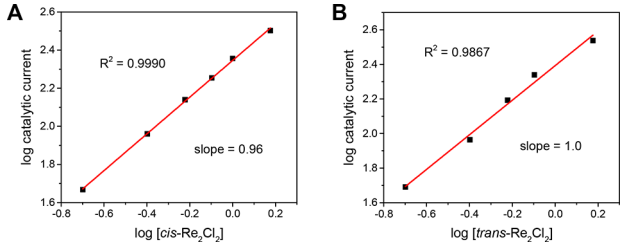

Figure 6. Catalyst concentration dependence for (A) *cis*-Re_2Cl_2 and (B) *trans*-Re_2Cl_2 in CO_2-saturated DMF/0.1 M Bu_4NPF_6 solutions. Glassy carbon disk; ν = 100 mV s^{-1}. Linear fits with slopes of 1 were obtained in log−log plots of catalytic current (μA) versus catalyst concentration (mM).

For both conformers, the data indicate a first-order dependence on [Re_2Cl_2] and a first-order dependence on [CO_2] in the rate-determining step, as expressed by the following rate law:

$$\text{rate} = -\frac{[CO_2]}{dt} = k_{cat}[Re_2Cl_2][CO_2]$$

It was not possible on the basis of reaction orders alone to distinguish between the reaction mechanisms of the *cis* and *trans* conformers. The log−log plots were critical for the correct kinetic analysis of these catalysts because plots of both catalytic current versus [*trans*-Re_2Cl_2] and catalytic current versus [*trans*-Re_2Cl_2]$^{1/2}$ gave reasonable linear fits (Figure S13). The log−log plots confirm that the reactions are first-order in catalyst with slopes of 1 (Figure 6).

Our initial inquiry regarding a half-order dependence on catalyst concentration, specifically for *trans*-Re_2Cl_2, emerged from a previous mechanistic study involving a dinuclear palladium complex, in which its polydentate phosphine ligand was designed to prevent cooperative, intramolecular CO_2 binding between active sites.[48] A half-order dependence on catalyst concentration was reported and explained by assuming the metal active sites operate independently of one another, such that only half of the complex is intimately involved in the rate-determining step.[48b] As rationalized, however, a first-order dependence would be expected. A square-root dependence on catalyst concentration is typically observed following rate-limiting dissociation of a dinuclear precatalyst that is in reversible equilibrium with the active form.[49,50]

Several plausible modes of reactivity with a dinuclear catalyst for CO_2 reduction are expected to yield a first-order dependence on the catalyst concentration: (1) both metal centers participate in the intramolecular activation, or binding, of CO_2 and its conversion; (2) only one metal center reacts with CO_2, while the other acts as a spectator; (3) only one metal center reacts with CO_2, while the other serves as an electron reservoir capable of intramolecular electron transfer; (4) both metal centers operate independently and react with one CO_2 molecule each. In cases 2 and 3, the metal fragment that does not bind CO_2 can be thought of more simply as (2) an elaborate ligand substituent of variable electronics depending on its redox state or (3) a pendant redox mediator that supplies electron(s) to the active site, neither of which would give a half-order dependence on the catalyst concentration.

■ CATALYTIC RATES AND FARADAIC EFFICIENCIES

With these results in hand, we sought to compare the catalytic rates of the *cis* and *trans* conformers along with Re(bpy)-$(CO)_3Cl$ and its anthracene-functionalized derivative, anthryl-Re. The quantity $(i_{cat}/i_p)^2$ can serve as a useful benchmark of catalytic activity that is proportional to the turnover frequency (TOF), as shown in eq 2, where ν is the scan rate, n_p is the number of electrons transferred in the noncatalytic Faradaic process, R is the ideal gas constant, T is the temperature (in K), and i_p is the peak current observed for the catalyst in the absence of substrate.[34,51]

$$\text{TOF} = k_{cat}[CO_2] = \frac{F\nu n_p^{\,3}}{RT}\left(\frac{0.4463}{n_{cat}}\right)^2\left(\frac{i_{cat}}{i_p}\right)^2 \quad (2)$$

The application of eq 2 requires steady-state behavior, which can often be established at sufficiently fast scan rates that avoid substrate depletion and give rise to a limiting catalytic current plateau. Linear-sweep voltammograms of *cis*-Re_2Cl_2 (1 mM), *trans*-Re_2Cl_2 (1 mM), and the mononuclear catalysts (2 mM) were conducted in DMF/0.1 M Bu_4NPF_6 solutions under argon and CO_2 as a function of the scan rate (Figure S14). While scan rate independence was not completely reached, estimated TOFs using eq 2 are plotted versus the scan rate in Figure S15, where TOFs of 35.3, 22.9, 11.1, and 19.2 s^{-1} were identified for *cis*-Re_2Cl_2, *trans*-Re_2Cl_2, Re(bpy)$(CO)_3Cl$, and anthryl-Re, respectively.

Alternatively, Costentin and Savéant's foot-of-the-wave analysis (FOWA)[46,52,53] can be applied to find intrinsic catalytic rates via eq 3:

DOI: 10.1021/acs.inorgchem.8b01775
Inorg. Chem. XXXX, XXX, XXX−XXX

$$\frac{i}{i_p} = \frac{2.24\sqrt{\frac{RT}{F\nu n_p^3}2k_{cat}[CO_2]}}{1 + \exp\left[\frac{F}{RT}(E - E_{cat/2})\right]} \quad (3)$$

This electroanalytical method provides access to a TOF maximum, in which the observed catalytic rate constant k_{cat} can be determined at the foot of the catalytic wave, where competing factors (i.e., substrate depletion, catalyst inhibition, or decomposition) are minimal. Indeed, scan rate-independent TOFs were obtained by FOWA (Figure S16). In eq 3, $E_{cat/2}$ is the half-wave potential of the catalytic wave. From the slope of the linear portion of a plot of i/i_p versus $1/\{1 + \exp[(F/RT)(E-E_{cat/2})]\}$, k_{cat} can be calculated.[54] The maximum TOF under saturation conditions is then found from TOF = $k_{cat}[CO_2]$.

The maximum TOFs determined via FOWA for the dinuclear catalysts (11.0 s^{-1}, *cis*-Re_2Cl_2; 4.4 s^{-1}, *trans*-Re_2Cl_2) are higher than that of the mononuclear parent catalyst (1.5 s^{-1}) at the same effective concentrations. Likewise, the *cis* conformer is considerably more active than its *trans* counterpart, consistent with the estimated TOFs from eq 2. With regard to anthryl-Re (4.1 s^{-1}), the pendant anthracene results in a higher TOF relative to unsubstituted Re(bpy)$(CO)_3$Cl, whereas very similar rates (via both electroanalytical equations) are observed relative to *trans*-Re_2Cl_2. Comparable TOFs of anthryl-Re and *trans*-Re_2Cl_2 are consistent with the isolated active sites of the dinuclear complex on opposite sides of the anthracene bridge. Notably, slow catalysis begins after the first overlapping one-electron reductions at around −1.9 V with the dinuclear catalysts, while no activity is observed until the second reduction at −2.1 V for the monomers.

Brønsted acids are frequently added to polar aprotic solvents to promote the proton-coupled reduction of CO_2. Indeed, significant enhancements in the electrocatalytic CO_2 reduction activity of mononuclear rhenium catalysts have been observed with various proton source additives.[13,55,56] The influence of four different acids [H_2O, methanol (MeOH), 2,2,2-trifluoroethanol (TFE), and phenol (PhOH)] on the CO_2 reduction activity of *cis*-Re_2Cl_2 in DMF was investigated (Figure S17). This selection of proton sources affords a good range of acidity, with the following pK_a values reported in dimethyl sulfoxide (DMSO):[57] 31.4 (H_2O),[58] 29.0 (MeOH),[58] 23.5 (TFE),[59] 18.0 (PhOH).[60] The catalyst *cis*-Re_2Cl_2 shows a decrease in the current upon addition of these acids. However, the onset of fast catalysis is significantly more positive after the addition of a proton source relative to anhydrous DMF. From cyclic voltammetry, added H_2O produces the most promising catalytic activity for CO_2 reduction with *cis*-Re_2Cl_2 of the four Brønsted acids investigated, taking into account its nominal activity under argon. Accordingly, the amount of added H_2O was optimized for *cis*-Re_2Cl_2 by plotting i_{cat} versus H_2O concentration where catalysis reached a maximum with 3 M H_2O (Figure S18). The catalytic activity of each catalyst in the presence of 3 M H_2O is shown in Figure 7 for comparison.

A thermodynamic potential of −0.73 V vs $Fc^{+/0}$ for the $2e^-/2H^+$ CO_2/CO couple in pure DMF has been determined via a thermochemical approach.[61] In the presence of a Brønsted acid, this standard potential shifts according to eq 4, in which the pK_a value of the acid must be taken into account.[61]

$$E = E^0_{CO_2/CO(DMF)} - 0.0592pK_a \quad (4)$$

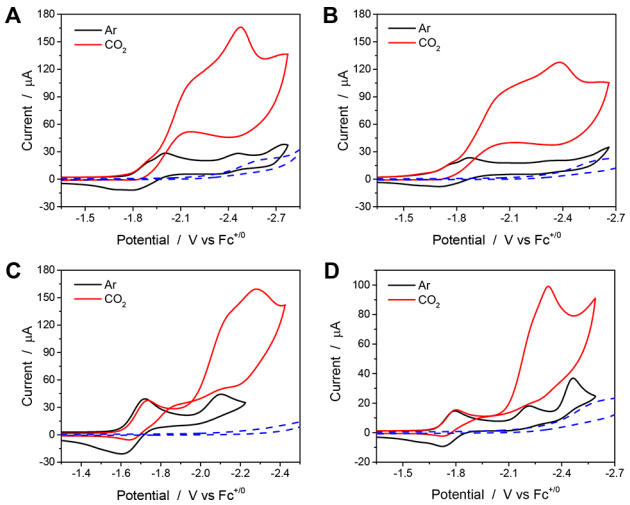

Figure 7. CVs of (A) 1 mM *cis*-Re_2Cl_2, (B) 1 mM *trans*-Re_2Cl_2, (C) 2 mM Re(bpy)$(CO)_3$Cl, and (D) 2 mM anthryl-Re with 3 M H_2O in DMF/0.1 M Bu_4NPF_6 under argon (black) and CO_2 (red). Glassy carbon disk; ν = 100 mV s^{-1}.

As previously described, carbonic acid (H_2CO_3, pK_a = 7.37) is more acidic than H_2O in DMF, so its pK_a was used in eq 4 to give an estimated reduction potential of −1.17 V for the CO_2/CO couple in DMF/H_2O solutions.[36] Using these standard potentials, a summary of the TOFs from anhydrous DMF and observed overpotentials from Figures 4 and 7, based on $E_{cat/2}$, is presented in Table 2. $E_{cat/2}$ is a reliable metric that corresponds to the steepest point, or nearly so, in the catalytic wave of the current−potential profile.[62] It is worth mentioning that overpotentials cited in Table 2 correspond to applied potentials and/or conditions that promote the $2e^-/2H^+$ reduction of CO_2 to CO + H_2O. To the best of our knowledge, a standard potential for the reductive disproportionation of CO_2 to CO + CO_3^{2-} has not been reported.

Controlled potential electrolyses were carried out to identify the products and Faradaic efficiencies in an airtight electrochemical cell using a glassy carbon rod working electrode and CO_2-saturated solutions. The applied potential (E_{appl}) corresponds to the potential at which the maximum current was observed in CVs taken in the same setup prior to electrolysis. Headspace gases and electrolytic solutions were analyzed by gas chromatography and ^{1}H NMR and FTIR spectroscopies.[63−65] CO was found to be the only detectable product under these conditions, where E_{appl} is −2.4 or −2.5 V (Table 3). No other products were observed. In addition to IR spectroscopy, titration with barium triflate was also conducted to investigate carbonate as a potential product. Formation of $BaCO_3$ was not apparent.[10,63,64] The absence of carbonate indicates that the dinuclear catalysts do not mediate reductive disproportionation of CO_2, i.e., $2CO_2 + 2e^- \rightarrow CO + CO_3^{2-}$ *at these potentials*, consistent with earlier results with Re(bpy)$(CO)_3$Cl in DMF solutions.[22] It is well-established that under anhydrous conditions protons can be generated by Hofmann degradation of the quaternary alkylammonium cation of the supporting electrolyte.[22,66] This degradation is thought to arise from a highly basic metal carboxylate intermediate that is capable of deprotonating the tetrabutylammonium ion,[66] consistent with IR stopped-flow measurements in the absence of an added proton source.[67]

DOI: 10.1021/acs.inorgchem.8b01775
Inorg. Chem. XXXX, XXX, XXX−XXX

Table 2. Summary of Electrocatalysis Obtained from Cyclic Voltammetry

catalyst	TOF (s^{-1}) eq 2	TOF (s^{-1}) eq 3	$E_{cat/2}(\eta)^a$	$E_{cat/2}(\eta)^b$
cis-Re_2Cl_2	35.3	11.0	−2.29 (1.56)	−2.09 (0.92)
trans-Re_2Cl_2	22.9	4.4	−2.34 (1.61)	−1.95 (0.78)
Re(bpy)$(CO)_3$Cl	11.1	1.5	−2.22 (1.49)	−2.04 (0.87)
anthryl-Re	19.2	4.1	−2.26 (1.53)	−2.18 (1.01)

[a]Anhydrous DMF. [b]DMF with 3 M H_2O. $E_{cat/2}$ is the potential at which the current is equal to $i_{cat/2}$. Overpotentials reported here were calculated from the expression $\eta = |E_{cat/2} - E^0_{CO_2/CO}|$.

Table 3. Summary of Controlled Potential Electrolyses and Faradaic Efficiencies for CO_2 Reduction under Various Conditions

catalyst	time (min)	E_{appl} (V)	charge passed (C)	CO (%)
cis-Re_2Cl_2	60	−2.5	1.52 ± 0.32	81 ± 1
trans-Re_2Cl_2	60	−2.5	0.60 ± 0.08	89 ± 6
Re(bpy)$(CO)_3$Cl	60	−2.5	1.17 ± 0.15	78 ± 10
cis-Re_2Cl_2 (3 M H_2O)	60	−2.4	0.96 ± 0.22	59 ± 5
trans-Re_2Cl_2 (3 M H_2O)	60	−2.4	1.01 ± 0.09	74 ± 1
Re(bpy)$(CO)_3$Cl (3 M H_2O)	60	−2.4	0.92 ± 0.29	65 ± 6
cis-Re_2Cl_2	180	−2.0	2.24 ± 0.37	52 ± 5
cis-Re_2Cl_2	600	−2.0	5.94 ± 0.82	52 ± 5
trans-Re_2Cl_2	180	−2.0	1.01 ± 0.12	49 ± 5
cis-Re_2Cl_2 (3 M H_2O)	600	−2.0	6.27 ± 0.03	47 ± 3
trans-Re_2Cl_2 (3 M H_2O)	600	−2.0	4.46 ± 0.11	49 ± 6

At lower applied potentials, Re(bpy)$(CO)_3$Cl is known to catalyze the reductive disproportionation of CO_2 through the so-called "one-electron pathway".[22] Following its one-electron reduction, the parent catalyst reduces CO_2 in a bimolecular process to give CO and CO_3^{2-}. In this mechanism, two singly reduced catalysts are proposed to bind CO_2 to generate a Re_2 carboxylate-bridged intermediate that undergoes insertion with a second equivalent of CO_2 before reductive disproportionation. Here, CO_2 acts as an oxide acceptor to facilitate a proton-independent conversion of CO_2 to CO. By inference, less basic intermediates are generated at these less reducing potentials and oxide transfer to CO_2 is favored over Hofmann degradation. We note that the hydrogen-bonded Re(bpy) dimers developed by Kubiak and co-workers also promote this bimolecular pathway with enhanced rates.[34]

In this context, we investigated the *cis* and *trans* conformers at applied potentials immediately following the first overlapping one-electron reductions. Controlled potential electrolyses were conducted in anhydrous DMF/0.1 M Bu_4NPF_6 as well as solutions containing 3 M H_2O. Unsurprisingly, *trans*-Re_2Cl_2 was found to catalyze the reductive disproportionation of CO_2 at an applied potential of −2.0 V in anhydrous DMF. Given its solid-state structure, catalytic activity analogous to that of Re(bpy)$(CO)_3$Cl was expected for the *trans* conformer and carbonate was identified as a coproduct by IR spectroscopy, with strong C−O stretching frequencies observed at ∼1450 and 1600 cm^{-1} (Figure 8A) and subsequent precipitation of $BaCO_3$ from DMF solutions.[64,68] Conversely, carbonate was not observed with *cis*-Re_2Cl_2. In order to bolster this result and ensure that carbonate is not simply sequestered in a stable species (i.e., bound between rhenium centers), long-term electrolyses were performed in which the evolved CO amounts to greater than two turnovers with respect to total moles of catalyst in solution. On this basis, *cis*-Re_2Cl_2 does not catalyze the reductive disproportionation of CO_2, consistent with the IR spectra in Figure 8B. Presumably, restricted rotation of the Re(bpy) fragments in *cis*-Re_2Cl_2 impedes the

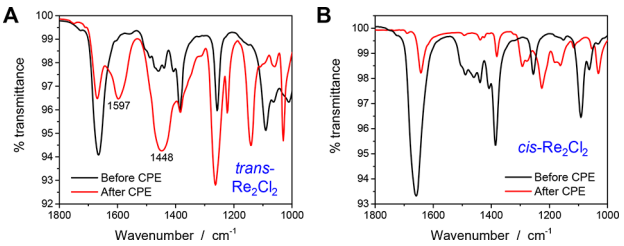

Figure 8. FTIR spectra of (A) *trans*-Re_2Cl_2 and (B) *cis*-Re_2Cl_2 samples before and after electrolysis. Electrolyzed solutions are evaporated to dryness and washed with dichloromethane to remove the Bu_4NPF_6 electrolyte. The resulting solid is analyzed.

CO_2 insertion step and favors protonation of the CO_2 adduct by slow Hofmann degradation.

With 3 M H_2O, at the lower applied potential (−2.0 V vs $Fc^{+/0}$), carbonate or bicarbonate is not produced by *cis*-Re_2Cl_2 or *trans*-Re_2Cl_2. Authentic samples of tetrabutylammonium carbonate and tetrabutylammonium bicarbonate were synthesized[68,69] and detected by FTIR using the established protocol and barium triflate titration to validate these results. Consistent with the enhanced catalysis at initial reductions of both Re_2 catalysts (Figure 7) and the concentration dependence in Figure S18, the addition of water clearly promotes the proton-coupled reduction of CO_2, i.e., $CO_2 + 2H^+ + 2e^- \rightarrow CO + H_2O$, at lower overpotentials. Representative charge-time profiles from electrolyses in DMF solutions are overlaid in Figure S19. Experiments were performed in duplicate, and the results are summarized in Table 3.

■ UV−VIS SPECTROELECTROCHEMISTRY

Additional insight into the electrocatalytic CO_2 reduction mechanisms of the *cis* and *trans* conformers was gained from UV−vis spectroelectrochemical (SEC) measurements. Data were collected stepwise at increasingly negative applied potentials under an argon atmosphere using a thin-layer cell with a "honeycomb" working electrode. Representative

DOI: 10.1021/acs.inorgchem.8b01775
Inorg. Chem. XXXX, XXX, XXX−XXX

absorption spectra versus time (Figure 9) are shown for *cis*-Re_2Cl_2 and *trans*-Re_2Cl_2.

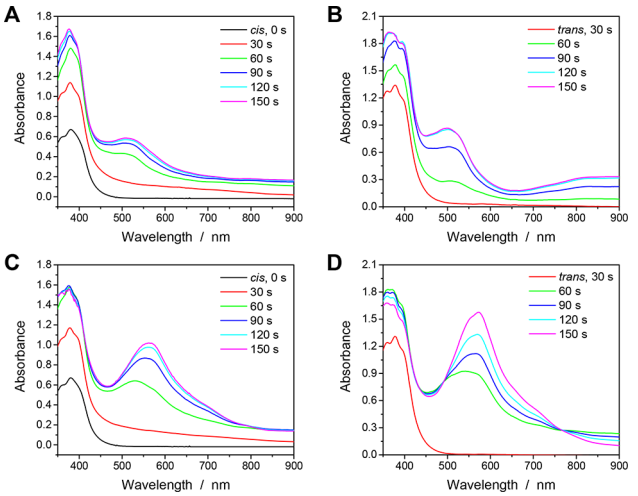

Figure 9. UV−vis spectroelectrochemistry with (A) 0.5 mM *cis*-Re_2Cl_2 at −1.7 V versus Ag/AgCl, (B) 0.5 mM *trans*-Re_2Cl_2 at −1.7 V versus Ag/AgCl, (C) 0.5 mM *cis*-Re_2Cl_2 at −2.0 V versus Ag/AgCl, (D) 0.5 mM *trans*-Re_2Cl_2 at −2.0 V versus Ag/AgCl in argon-saturated DMF/0.1 M Bu_4NPF_6 solutions.

At an applied potential of −1.7 V versus Ag^+, both *cis*-Re_2Cl_2 and *trans*-Re_2Cl_2 catalysts display a new absorption peak at 517 nm, consistent with the one-electron-reduced species.[70] The terminology used here refers to reduction at a single rhenium site to facilitate a comparison with earlier studies on mononuclear catalysts. The catalysts have been reduced by two electrons in total. At a more negative applied potential of −2.0 V versus Ag^+, absorption bands at 562 nm (*cis*-Re_2Cl_2) and 570 nm (*trans*-Re_2Cl_2) appear, indicative of the two-electron-reduced species.[7]

Upon closer inspection of the absorption spectra obtained with E_{appl} = −1.7 V versus Ag^+, a broad band centered around 850 nm also emerges for the *trans* conformer. This feature is characteristic of a Re−Re-bonded dimer,[7] presumably a Re_4 species in this case formed from 2 equiv of *trans*-Re_2Cl_2. Characteristic absorption features of a Re−Re dimer, however, were not observed in experiments with *cis*-Re_2Cl_2. We reasoned that an added benefit of the rigid anthracene backbone is constraining the metal centers from Re−Re bond formation, a known deactivation pathway.

DFT calculations were conducted to probe the likelihood of forming the neutral Re−Re dimer or its one-electron-reduced product with *cis*-Re_2Cl_2. Optimized geometries are shown in Figure 10. Calculated distances between rhenium centers are 3.38 Å for the neutral species and 3.52 Å for the radical anion. Solid-state structures of the corresponding dimers prepared from $Re(bpy)(CO)_3Cl$ reduction have been characterized by X-ray crystallography.[27] A Re−Re bond distance of 3.0791(13) Å was found in the neutral dimer and a longer distance of 3.1574(6) Å was determined in the reduced dimer.[27] Given the calculated intermetallic distances for the anthracene-based catalyst in conjunction with the SEC data, the Re−Re-bonded dimer is likely inaccessible following the reduction of *cis*-Re_2Cl_2 or is limited to a transient interaction. These results are consistent with the improved stability observed in controlled potential electrolyses with *cis*-Re_2Cl_2.

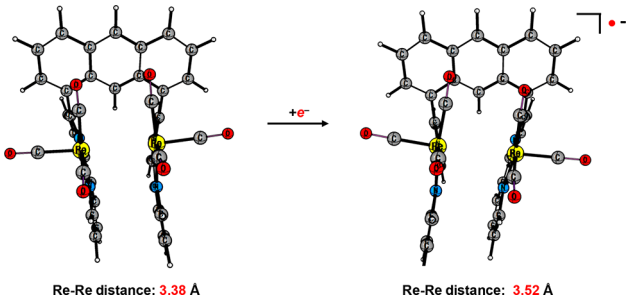

Figure 10. Possible intermediates following reduction and chloride dissociation from *cis*-Re_2Cl_2. DFT-optimized structures of a neutral dinuclear rhenium species and its one-electron-reduced radical anion.

It is clear from the structure of *trans*-Re_2Cl_2 and the observed reactivity that catalysis occurs by well-established pathways known for $Re(bpy)(CO)_3Cl$ (catalytic cycles are shown in Figure S20), including the "one-electron" bimolecular reductive disproportionation mechanism at applied potentials just after the initial overlapping one-electron reductions of the Re_2 complex under anhydrous conditions. Carbonate is a coproduct of this bimolecular pathway for *trans*-Re_2Cl_2. However, in the presence of 3 M H_2O or at more negative potentials, CO_2-to-CO conversion occurs but with H_2O as the coproduct.

Different behavior is observed for *cis*-Re_2Cl_2. Proposed catalytic cycles for the two applied potential regimes at −2.0 and ≤−2.4 V are given in Figures 11 and S21, respectively. In contrast to the mononuclear catalyst and *trans*-Re_2Cl_2, the *cis* conformer does not generate carbonate at applied potentials immediately following the initial overlapping one-electron reductions. This difference in reactivity is presumably a consequence of the proximal active sites being confined by

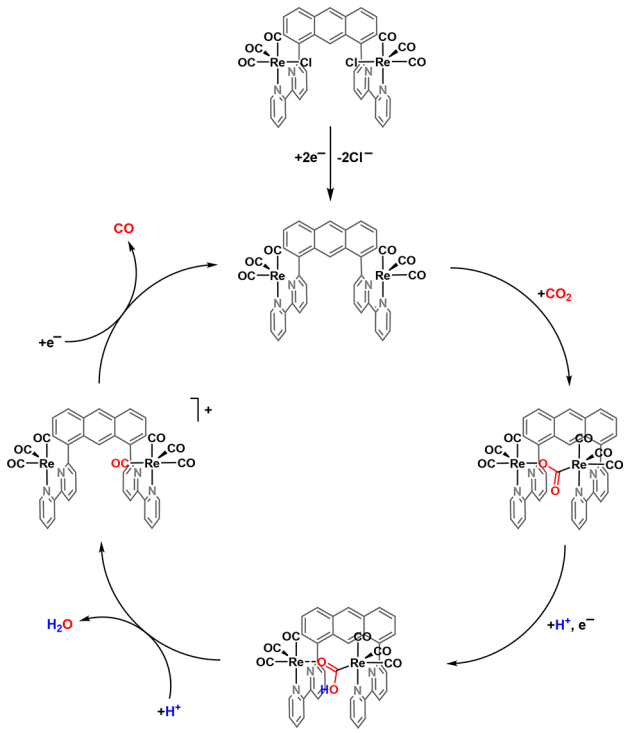

Figure 11. Proposed mechanism for *cis*-Re_2Cl_2 at E_{appl} = −2.0 V versus $Fc^{+/0}$ in DMF/0.1 M Bu_4NPF_6.

DOI: 10.1021/acs.inorgchem.8b01775
Inorg. Chem. XXXX, XXX, XXX−XXX

hindered rotation about the anthracene bridge. With this catalyst, CO_2 is unable to act as an oxide acceptor by CO_2 insertion into the Re−O bond of the bridging carboxylate; instead, CO_2 reduction is governed by protonation via Hofmann degradation of the supporting electrolyte. Along these lines, Kubiak's dynamic hydrogen-bonded dinuclear system mediates reductive disproportionation at low applied potentials, analogous to the "one-electron" pathway of $Re(bpy)(CO)_3Cl$ and consistent with its flexibility to accommodate a CO_2 insertion step.[34] The proposed mechanism of *cis*-Re_2Cl_2 at more negative potentials (Figure S21) is similar to Figure 11 but with fast catalysis coinciding with further reduction of the catalyst.

■ CONCLUSION

We have described a novel ligand platform that gives access to isolable *cis* and *trans* conformers comprised of two rhenium active sites. Indeed, the conformers were purified by silica gel chromatography and characterized. Consistent with its NMR spectra, a crystal structure of *trans*-Re_2Cl_2 confirmed the asymmetric orientation of rhenium sites on opposite sides of the anthracene bridge. In contrast, the combined data (^{1}H NMR, FTIR, and reactivity studies) indicate that the *cis* conformer is a symmetric species in which the rhenium sites are on the same side of the anthracene backbone with their chloro ligands directed toward one another. Both Re_2 compounds are active electrocatalysts for reducing CO_2 to CO. From mechanistic studies, a pathway involving bimetallic CO_2 activation and conversion was identified for *cis*-Re_2Cl_2, whereas well-established single-site and bimolecular pathways, analogous to that of $Re(bpy)(CO)_3Cl$, were observed for *trans*-Re_2Cl_2.

The catalytic rates were measured by cyclic voltammetry for *cis*-Re_2Cl_2, *trans*-Re_2Cl_2, $Re(bpy)(CO)_3Cl$, and anthryl-Re with estimated TOFs of 35.3, 22.9, 11.1, and 19.2 s^{-1}, respectively. The maximum TOFs of *trans*-Re_2Cl_2 and anthryl-Re (at twice the concentration) are approximately equal, showing the effect of the pendant anthracene on catalytic activity in comparison to $Re(bpy)(CO)_3Cl$ and with each having single-site reactivity. On the other hand, the *cis* conformer clearly outperforms the *trans* conformer in terms of catalytic rate and stability, indicating that the structure of *cis*-Re_2Cl_2 enables improved performance. Indeed, a change in mechanism is observed at low applied potentials in anhydrous conditions where carbonate is not formed as a coproduct. Synergistic catalysis by cooperative active sites in *cis*-Re_2Cl_2 is hypothesized. SEC measurements indicate that *cis*-Re_2Cl_2 does not form a deactivated Re−Re-bonded species. The catalyst structure delivers a unique form of protection for catalyst longevity because *intermolecular* deactivation pathways are limited by the cofacial arrangement of active sites, while the rigid anthracene backbone prevents *intramolecular* Re−Re bond formation.

The *cis* and *trans* conformers reported here exhibit distinct mechanisms for electrochemical CO_2-to-CO conversion. Photocatalytic CO_2 reduction combined with photophysical studies exploring the role of anthracene as a pendant organic chromophore is in progress.

■ EXPERIMENTAL SECTION

Materials and Methods. Unless otherwise noted, all synthetic manipulations were performed under a dinitrogen atmosphere using standard Schlenk techniques or in an MBraun glovebox. Toluene was dried with a Pure Process Technology solvent purification system. Anhydrous *N*,*N*-dimethylformamide (DMF) was purchased from Alfa Aesar and packaged under argon in ChemSeal bottles. The rhenium precursor $Re(CO)_5Cl$ was purchased from Strem and stored in the glovebox. All other chemicals were reagent- or ACS-grade, purchased from commercial vendors, and used without further purification. ^{1}H and ^{13}C NMR spectra were obtained using a Bruker Advance DRX-500 spectrometer operating at 500 MHz (^{1}H) or 126 MHz (^{13}C). Spectra were calibrated to residual protiated solvent peaks; chemical shifts are reported in ppm. Electrospray ionization mass spectrometry (ESI-MS) spectra were obtained with a Waters SYNAPT HDMS Q-TOF mass spectrometer. UV−vis spectra were recorded on an Agilent/Hewlett-Packard 8453 UV−vis spectrophotometer with a diode-array detector. IR spectra were obtained on an Agilent Technologies Cary 600 series FTIR spectrometer equipped with a PIKE GladiATR accessory.

Electrochemical Measurements. Electrochemistry was performed with a Bioanalytical Systems, Inc. (BASi), Epsilon potentiostat. Cyclic voltammetry studies employed a three-electrode cell equipped with a glassy carbon disk (3 mm diameter) working electrode, a platinum wire counter electrode, and a silver wire quasi-reference electrode that was referenced using ferrocene as an internal standard at the end of the experiments. Electrochemistry was conducted in anhydrous DMF containing 0.1 M Bu_4NPF_6 supporting electrolyte. Solutions for cyclic voltammetry were thoroughly degassed with argon or CO_2 before data collection. All CVs were cycled from the most positive potential to the most negative potential and back.

Controlled potential electrolyses were carried out in a three-neck glass cell with a glassy carbon rod (2 mm diameter, type 2, Alfa Aesar) working electrode, a silver wire quasi-reference electrode, and a platinum mesh (2.5 cm^2 area, 150 mesh) counter electrode that was separated from the other electrodes in an isolation chamber comprised of a fine glass frit. Solutions were degassed with CO_2 for 30 min before data collection. The applied potential values were determined by cyclic voltammetry before controlled potential electrolysis was performed. Evolved gases during electrolysis measurements were quantified by gas chromatographic analysis of the headspace samples using an Agilent 7890B gas chromatograph and an Agilent PorapakQ (6 ft length and $^1/_8$ in. o.d.) column. CO was measured using a flame ionization detector equipped with a methanizer, while dihydrogen was quantified at the thermal conductivity detector. Constant stirring was maintained during electrolysis. Integrated gas peaks were quantified with calibration curves obtained from known standards purchased from BuyCalGas.com. From the experimental amount of product formed during electrolysis, the Faradaic efficiencies were calculated against the theoretical amount of product possible based on the accumulated charge passed and the stoichiometry of the reaction.

UV−vis SEC measurements were conducted with a commercial "honeycomb" thin-layer SEC cell from Pine Research Instrumentation, employing a gold working electrode, a silver wire quasi-reference electrode, and a platinum wire counter electrode.

X-ray Crystallography. Single crystals were coated with Paratone-N hydrocarbon oil and mounted on the tip of a MiTeGen micromount. The temperature was maintained at 100 K with an Oxford Cryostream 700 during data collection at the X-ray Crystallography Facility, Department of Chemistry and Biochemistry, University of Mississippi. Samples were irradiated with Mo Kα radiation with λ = 0.71073 Å using a Bruker Smart APEX II diffractometer equipped with a Microfocus Sealed Source (Incoatec IμS) and APEX-II detector. The Bruker *APEX2*, version 2009.1, software package was used to integrate raw data, which were corrected for Lorentz and polarization effects.[71] A semiempirical absorption correction (*SADABS*) was applied.[72] The structure was solved using direct methods and refined by least-squares refinement on F^2 and standard difference Fourier techniques using *SHELXL*.[73] The thermal parameters for all non-hydrogen atoms were refined anisotropically, and hydrogen atoms were included at ideal positions. Poorly resolved outer-sphere DMF molecules could not be modeled successfully in

DOI: 10.1021/acs.inorgchem.8b01775
Inorg. Chem. XXXX, XXX, XXX−XXX

the difference map. The data were treated with the *SQUEEZE* procedure in *PLATON*;[74] details are provided in the CIF file.

Computational Methods. All calculations were performed in *Gaussian 09*.[75] All energies discussed in this work contain zero-point-energy corrections.[76] Global minima of the *cis* and *trans* conformers were located using DFT and the ωB97X-D[76] functional.[77] The 6-311+G* basis set was used for all coordinating atoms, which include CO. The 6-311G* basis was used for all hydrogen and carbon atoms of the ligand manifold. LanL2TZ(f) was used for the two rhenium atoms. The minima were confirmed by calculating the harmonic vibrational frequencies and finding all real values. To obtain a structure close to the transition state (TS) of conformational isomerization (via rotation), an initial relaxed scan was performed using semiempirical PM6 and parametrized by the dihedral angle C(14)−C(15)−C(23)−N(39) or C(6)−C(5)−C(29)−N(40) for TS1 and TS2, respectively, as labeled in Figure S5. From these scans, the maximum was used as the starting point for a TS optimization using the Berny algorithm at the level of theory and basis sets mentioned previously.

Structural optimization and IR spectral calculations were performed using the BP86-D3/def2-TZVP functional−basis set combination with Beck's and Johnston's dispersion corrections. The rhenium atoms were described with the LanL2TZ(f) effective core potential with the added polarization function. These calculations also included DMF solvent-induced corrections using the COSMO solvation model. Frequency analysis confirmed the global minima.

Global minima for the Re−Re dimers (Figure 10) were found using the ωB97X-D functional with basis sets LanL2TZ(f) for rhenium atoms and 6-31++G* for all light atoms. An ultrafine numerical integration grid was employed for both species. Cartesian coordinates and energies are given in Tables S2−S11.

Synthetic Procedures. Re(bpy)$(CO)_3$Cl was prepared as previously described.[78] Ligand precursors 6-bromo-2,2′-bipyridine[79] and 1,8-bis(neopentylglycolatoboryl)anthracene[38] were prepared according to literature procedures.

1,8-Bis(2,2′-bipyridine)anthracene (1). In an oven-dried, two-neck, round-bottomed flask were added 1,8-bis-(neopentylglycolatoboryl)anthracene (1.0 g, 2.49 mmol), 6-bromo-2,2′-bipyridine (1.4 g, 5.97 mmol), and $Pd(PPh_3)_4$ (0.172 g, 6 mol %) under an inert atmosphere. Degassed toluene (50 mL), ethanol (5 mL), and 2 M aqueous K_2CO_3 (5 mL) were added to the reaction vessel under dinitrogen and refluxed for 2 days. After cooling to room temperature, 25 mL of saturated aqueous NH_4Cl and 25 mL of H_2O were added to the mixture. The crude product was extracted with dichloromethane and purified by silica gel chromatography (1:1 hexanes/ethyl acetate) to yield a pure product (1.04 g, 86%). ^{1}H NMR (500 MHz, DMSO-d_6): δ 9.80 (s, 1H), 8.83 (s, 1H), 8.62 (ddd, *J* = 4.7, 1.8, and 0.9 Hz, 2H), 8.27 (d, *J* = 8.4 Hz, 2H), 7.98 (dt, *J* = 7.8 and 1.0 Hz, 2H), 7.83 (dq, *J* = 7.9 and 1.0 Hz, 2H), 7.78−7.73 (m, 4H), 7.71−7.65 (m, 4H), 7.57 (td, *J* = 7.7 and 1.8 Hz, 2H), 7.33 (ddt, *J* = 6.9, 4.8, and 1.1 Hz, 2H). ^{13}C NMR (126 MHz, DMSO-d_6): δ 157.60, 154.89, 154.52, 149.01, 137.99, 137.85, 137.01, 131.55, 129.14, 129.06, 127.38, 126.91, 125.50, 124.92, 123.84, 123.61, 119.96, 118.61. ESI-MS. Calcd for [**1** + H^+] (M^+): *m/z* 487.2. Found: *m/z* 487.2.

1,8-Bis(2,2′-bipyridine)anthracene(Re(CO)$_3$Cl)$_2$ (Re$_2$Cl$_2$). To an oven-dried, two-neck, round-bottomed flask were added 1,8-bis-(2,2′-bipyridine)anthracene (100 mg, 0.205 mmol) and $Re(CO)_5Cl$ (148 mg, 0.41 mmol) under an inert atmosphere. Anhydrous toluene (5 mL) was added, and the reaction mixture was refluxed overnight. The mixture was cooled to room temperature, and the precipitate was collected by filtration with a glass frit and washed with toluene and diethyl ether several times. The crude product was purified by silica gel chromatography with gradient elution from dichloromethane to 2:3 acetone/dichloromethane using a Biotage automated flash purification system to give pure compounds, *cis*-Re_2Cl_2 (41% yield) and *trans*-Re_2Cl_2 (20% yield).

cis-Re$_2$Cl$_2$. ^{1}H NMR (500 MHz, DMSO-d_6): δ 9.04 (d, *J* = 5.4 Hz, 2H), 8.87 (s, 1H), 8.77 (d, *J* = 8.3 Hz, 2H), 8.68 (d, *J* = 8.1 Hz, 2H), 8.39 (d, *J* = 8.5 Hz, 2H), 8.35 (t, *J* = 7.9 Hz, 2H), 7.90 (t, *J* = 7.9 Hz, 2H), 7.83 (s, 1H), 7.74 (m, 4H), 7.61 (d, *J* = 7.6 Hz, 2H), 7.54 (d, *J* = 6.6 Hz, 2H). ^{13}C NMR (126 MHz, DMF-d_7): δ 199.47, 195.09, 195.07, 161.87, 158.22, 157.57, 154.10, 141.11, 140.77, 133.41, 131.90, 131.57, 131.42, 131.02, 128.77, 128.71, 128.48, 128.32, 126.82, 126.10, 125.93, 124.94, 124.04. ATR-FTIR: ν(CO) at 2015, 1915 (with shoulder at 1924), and 1871 cm^{-1}. ESI-MS. Calcd for [*cis*-Re_2Cl_2 + Cs^+] (M^+): *m/z* 1230.9. Found: *m/z* 1230.9.

trans-Re$_2$Cl$_2$. ^{1}H NMR (500 MHz, DMSO-d_6): δ 9.01 (d, *J* = 5.4 Hz, 1H), 8.98 (d, *J* = 5.4 Hz, 1H), 8.87 (s, 1H), 8.77 (d, *J* = 8.3 Hz, 1H), 8.73 (d, *J* = 8.2 Hz, 1H), 8.61 (d, *J* = 8.1 Hz, 1H), 8.57 (d, *J* = 8.1 Hz, 1H), 8.42 (t, *J* = 8.0 Hz, 1H), 8.39−8.32 (m, 3H), 8.02 (t, *J* = 7.9 Hz, 1H), 7.83 (t, *J* = 6.6 Hz, 1H), 7.77−7.68 (m, 3H), 7.65 (d, *J* = 7.1 Hz, 2H), 7.53 (t, *J* = 7.8 Hz, 1H), 7.49 (d, *J* = 6.8 Hz, 1H), 7.44 (d, *J* = 7.7 Hz, 1H), 7.33 (s, 1H). ^{13}C NMR (126 MHz, DMF-d_7): δ 199.36, 198.83, 195.14, 194.84, 191.95, 190.96, 162.48, 162.45, 157.90, 157.83, 157.60, 157.06, 154.20, 154.09, 141.80, 141.36, 141.12, 140.91, 140.59, 139.59, 133.31, 133.22, 131.91, 131.60, 131.50, 130.92, 130.57, 130.37, 129.28, 128.81, 128.61, 128.51, 126.67, 126.12, 126.01, 125.90, 124.42, 124.39, 123.92. ATR-FTIR: ν(CO) at 2015 and 1891 cm^{-1}. ESI-MS. Calcd for [*trans*-Re_2Cl_2 + Cs^+] (M^+): *m/z* 1230.9. Found: *m/z* 1230.9.

1-(2,2′-Bipyridine)anthracene (2). To an oven-dried, two-neck, round-bottomed flask were added 1-(neopentylglycolatoboryl)-anthracene (1.0 g, 3.46 mmol), 6-bromo-2,2′-bipyridine (1.0 g, 4.15 mmol), and $Pd(PPh_3)_4$ (0.2 g, 5 mol %) under an inert atmosphere. Degassed toluene (50 mL), ethanol (5 mL), and 2 M aqueous solution of K_2CO_3 (5 mL) were added to the reaction vessel under dinitrogen and refluxed for 2 days. After cooling to room temperature, 25 mL of saturated NH_4Cl and 25 mL of H_2O were added to the mixture. The crude product was extracted with dichloromethane and purified by silica gel chromatography (5:1 hexanes/ethyl acetate) to yield a pure product (0.6 g, 52%). ^{1}H NMR (500 MHz, DMSO-d_6): δ 8.84 (s, 1H), 8.76 (dd, *J* = 88.9 and 4.7 Hz, 1H), 8.72 (s, 1H), 8.52 (d, *J* = 7.8 Hz, 1H), 8.41 (d, *J* = 8.0 Hz, 1H), 8.24 (d, *J* = 8.4 Hz, 1H), 8.18 (t, *J* = 7.8 Hz, 1H), 8.13 (d, *J* = 8.5 Hz, 1H), 8.00 (d, *J* = 8.4 Hz, 1H), 7.93 (td, *J* = 7.8 and 1.6 Hz, 1H), 7.85 (d, *J* = 7.6 Hz, 1H), 7.73 (d, *J* = 6.5 Hz, 1H), 7.66 (dd, 1H), 7.58−7.52 (m, 1H), 7.51−7.44 (m, 2H). ^{13}C NMR (126 MHz, DMSO-d_6): δ 158.47, 155.82, 155.49, 149.84, 138.87, 138.32, 137.89, 132.16, 131.98, 131.49, 129.73, 129.41, 129.06, 128.26, 127.78, 127.13, 126.43, 126.26, 125.69, 125.50, 124.86, 124.79, 121.07, 119.57. ESI-MS. Calcd for [**2** + H^+] (M^+): *m/z* 333.1. Found: *m/z* 333.1.

[1-(2,2′-Bipyridine)anthracene][Re(CO)$_3$Cl] (anthryl-Re). To an oven-dried, two-neck, round-bottomed flask were added 1-(2,2′-bipyridine)anthracene (100 mg, 0.300 mmol) and $Re(CO)_5Cl$ (109 mg, 0.300 mmol) under an inert atmosphere. Anhydrous toluene (5 mL) was added, and the reaction mixture was refluxed overnight. The mixture was cooled to room temperature, and the precipitate was collected by filtration with a glass frit and washed with toluene and diethyl ether several times. A pure product was obtained by crystallization from dichloromethane/hexanes (161 mg, 84%). Two conformers are present by ^{1}H NMR with slow rotation observed at room temperature. ESI-MS. Calcd for [anthryl-Re + Cs^+] (M^+): *m/z* 770.9453. Found: *m/z* 770.9452. Elem anal. Calcd for $C_{28}H_{16}N_2O_4Re{\cdot}1.5H_2O$: C, 48.76; H, 2.88; N, 4.21. Found: C, 49.09; H, 2.88; N, 4.22.

■ ASSOCIATED CONTENT

Supporting Information

The Supporting Information is available free of charge on the ACS Publications website at DOI: 10.1021/acs.inorgchem.8b01775.

Structures of seven possible isomers, ^{1}H NMR, experimental and theoretical IR spectra, calculated energy barrier, CVs, plots of i/i_p from linear sweep voltammograms, plot of TOF versus scan rate, concentration dependence, accumulated charge versus

DOI: 10.1021/acs.inorgchem.8b01775
Inorg. Chem. XXXX, XXX, XXX−XXX

time, catalytic cycles, crystallographic data, and Cartesian coordinates (PDF)

Accession Codes

CCDC 1578651 contains the supplementary crystallographic data for this paper. These data can be obtained free of charge via www.ccdc.cam.ac.uk/data_request/cif, or by emailing data_request@ccdc.cam.ac.uk, or by contacting The Cambridge Crystallographic Data Centre, 12 Union Road, Cambridge CB2 1EZ, UK; fax: +44 1223 336033.

■ AUTHOR INFORMATION

Corresponding Author

*E-mail: jwjurss@olemiss.edu.

ORCID

Winston C. Pitts: 0000-0001-8964-8441

Frank R. Fronczek: 0000-0001-5544-2779

Jonah W. Jurss: 0000-0002-2780-3415

Author Contributions

‡Contributed equally.

Notes

The authors declare no competing financial interest.

■ ACKNOWLEDGMENTS

We thank the University of Mississippi for generous start-up funds and a seed grant from the National Science Foundation (Grant OIA-1539035). The computational work is supported by the Mississippi Center for Supercomputing Research and the National Science Foundation (Grant CHE-1338056). We also thank Dr. Javier Concepcion for helpful discussions and Dr. Steven Davis and Sarah Johnson for guidance on the DFT calculations.

■ REFERENCES

(1) Lewis, N. S.; Nocera, D. G. Powering the planet: Chemical challenges in solar energy utilization. *Proc. Natl. Acad. Sci. U. S. A.* **2006**, *103*, 15729−15735.

(2) (a) Feely, R. A.; Sabine, C. L.; Lee, K.; Berelson, W.; Kleypas, J.; Fabry, V. J.; Millero, F. J. Impact of anthropogenic CO_2 on the $CaCO_3$ system in the oceans. *Science* **2004**, *305*, 362−366. (b) Houghton, J. Global warming. *Rep. Prog. Phys.* **2005**, *68*, 1343−1403. (c) IPCC. *Climate Change 2014: Synthesis Report. Contribution of Working Groups I, II and III to the Fifth Assessment Report of the Intergovernmental Panel on Climate Change*; Core Writing Team,-Pachauri, R. K., Meyer, L. A., Eds.; IPCC: Geneva, Switzerland, 2014; 151 pp.

(3) Concepcion, J. J.; House, R. L.; Papanikolas, J. M.; Meyer, T. J. Chemical approaches to artificial photosynthesis. *Proc. Natl. Acad. Sci. U. S. A.* **2012**, *109*, 15560−15564.

(4) (a) Benson, E. E.; Kubiak, C. P.; Sathrum, A. J.; Smieja, J. M. Electrocatalytic and homogeneous approaches to conversion of CO_2 to liquid fuels. *Chem. Soc. Rev.* **2009**, *38*, 89−99. (b) Yui, T.; Tamaki, Y.; Sekizawa, K.; Ishitani, O. Photocatalytic reduction of CO_2: from molecules to semiconductors. *Top. Curr. Chem.* **2011**, *303*, 151−184. (c) Finn, C.; Schnittger, S.; Yellowlees, L. J.; Love, J. B. Molecular approaches to the electrochemical reduction of carbon dioxide. *Chem. Commun.* **2012**, *48*, 1392−1399. (d) Appel, A. M.; Bercaw, J. E.; Bocarsly, A. B.; Dobbek, H.; DuBois, D. L.; Dupuis, M.; Ferry, J. G.; Fujita, E.; Hille, R.; Kenis, P. J. A.; Kerfeld, C. A.; Morris, R. H.; Peden, C. H. F.; Portis, A. R.; Ragsdale, S. W.; Rauchfuss, T. B.; Reek, J. N. H.; Seefeldt, L. C.; Thauer, R. K.; Waldrop, G. L. Frontiers, opportunities, and challenges in biochemical and chemical catalysis of CO_2 fixation. *Chem. Rev.* **2013**, *113*, 6621−6658. (e) Kang, P.; Chen, Z.; Brookhart, M.; Meyer, T. J. Electrocatalytic reduction of carbon dioxide: Let the molecules do the work. *Top. Catal.* **2015**, *58*, 30−45. (f) Takeda, H.; Cometto, C.; Ishitani, O.; Robert, M. Electrons, photons, protons, and earth-abundant metal complexes for molecular catalysis of CO_2 reduction. *ACS Catal.* **2017**, *7*, 70−88. (g) Francke, R.; Schille, B.; Roemelt, M. Homogeneously catalyzed electroreduction of carbon dioxide − methods, mechanisms, and catalysts. *Chem. Rev.* **2018**, *118*, 4631−4701.

(5) (a) Hawecker, J.; Lehn, J.-M.; Ziessel, R. Efficient photochemical reduction of CO_2 to CO by visible light irradiation of systems containing $Re(bipy)(CO)_3X$ or $Ru(bipy)_3^{2+}$-Co^{2+} combinations as homogeneous catalysts. *J. Chem. Soc., Chem. Commun.* **1983**, 536−538. (b) Hawecker, J.; Lehn, J.-M.; Ziessel, R. Electrocatalytic reduction of carbon dioxide mediated by $Re(bipy)(CO)_3Cl$ (bipy = 2,2′-bipyridine). *J. Chem. Soc., Chem. Commun.* **1984**, 328−330. (c) Hawecker, J.; Lehn, J.-M.; Ziessel, R. Photochemical and electrochemical reduction of carbon dioxide to carbon monoxide mediated by (2,2′-bipyridine)tricarbonylchlororhenium(I) and related complexes as homogeneous catalysts. *Helv. Chim. Acta* **1986**, *69*, 1990−2012.

(6) Johnson, F. P. A.; George, M. W.; Hartl, F.; Turner, J. J. Electrocatalytic reduction of CO_2 using the complexes $[Re(bpy)(CO)_3L]^n$ (n = + 1, L = $P(OEt)_3$, CH_3CN; n = 0, L = Cl^-, Otf^-; bpy = 2,2′-bipyridine; Otf^- = CF_3SO_3) as catalyst precursors: Infrared spectroelectrochemical investigation. *Organometallics* **1996**, *15*, 3374−3387.

(7) Breikss, A. I.; Abruña, H. D. Electrochemical and mechanistic studies of $[Re(CO)_3(dmbpy)Cl]$ and their relation to the catalytic reduction of CO_2. *J. Electroanal. Chem. Interfacial Electrochem.* **1986**, *201*, 347−358.

(8) Kurz, P.; Probst, B.; Spingler, B.; Alberto, R. Ligand variations in $[ReX(diimine)(CO)_3]$ complexes: Effects on photocatalytic CO_2 reduction. *Eur. J. Inorg. Chem.* **2006**, *2006*, 2966−2974.

(9) Smieja, J. M.; Kubiak, C. P. Re(bipy-tBu)$(CO)_3$Cl-improved catalytic activity for reduction of carbon dioxide: IR-spectroelectrochemical and mechanistic studies. *Inorg. Chem.* **2010**, *49*, 9283−9289.

(10) Machan, C. W.; Chabolla, S. A.; Kubiak, C. P. Reductive disproportionation of carbon dioxide by an alkyl-functionalized pyridine monoamine Re(I) fac-tricarbonyl electrocatalyst. *Organometallics* **2015**, *34*, 4678−4683.

(11) Stanton, C. J., III; Machan, C. W.; Vandezande, J. E.; Jin, T.; Majetich, G. F.; Schaefer, H. F., III; Kubiak, C. P.; Li, G.; Agarwal, J. Re(I) NHC complexes for electrocatalytic conversion of CO_2. *Inorg. Chem.* **2016**, *55*, 3136−3144.

(12) Huckaba, A. J.; Sharpe, E. A.; Delcamp, J. H. Photocatalytic reduction of CO_2 with Re-Pyridyl-NHCs. *Inorg. Chem.* **2016**, *55*, 682−690.

(13) Liyanage, N. P.; Dulaney, H. A.; Huckaba, A. J.; Jurss, J. W.; Delcamp, J. H. Electrocatalytic reduction of CO_2 to CO with Re-Pyridyl-NHCs: Proton source influence on rates and product selectivities. *Inorg. Chem.* **2016**, *55*, 6085−6094.

(14) Ching, H. Y. V.; Wang, X.; He, M.; Perujo Holland, N.; Guillot, R.; Slim, C.; Griveau, S.; Bertrand, H. C.; Policar, C.; Bedioui, F.; Fontecave, M. Rhenium complexes based on 2-pyridyl-1,2,3-triazole ligands: A new class of CO_2 reduction catalysts. *Inorg. Chem.* **2017**, *56*, 2966−2976.

(15) Sung, S.; Kumar, D.; Gil-Sepulcre, M.; Nippe, M. Electrocatalytic CO_2 reduction by imidazolium-functionalized molecular catalysts. *J. Am. Chem. Soc.* **2017**, *139*, 13993−13996.

(16) Nganga, J. K.; Samanamu, C. R.; Tanski, J. M.; Pacheco, C.; Saucedo, C.; Batista, V. S.; Grice, K. A.; Ertem, M. Z.; Angeles-Boza, A. M. Electrochemical reduction of CO_2 catalyzed by Re(pyridine-oxazoline)$(CO)_3$Cl complexes. *Inorg. Chem.* **2017**, *56*, 3214−3226.

(17) Nakada, A.; Ishitani, O. Selective electrocatalysis of a water-soluble rhenium(I) complex for CO_2 reduction using water as an electron donor. *ACS Catal.* **2018**, *8*, 354−363.

(18) (a) Ha, E.-G.; Chang, J.-A.; Byun, S.-M.; Pac, C.; Jang, D.-M.; Park, J.; Kang, S. O. High-turnover visible-light photoreduction of CO_2 by a Re(I) complex stabilized on dye-sensitized TiO_2. *Chem. Commun.* **2014**, *50*, 4462−4464. (b) Won, D.-I.; Lee, J.-S.; Ji, J.-M.;

DOI: 10.1021/acs.inorgchem.8b01775
Inorg. Chem. XXXX, XXX, XXX−XXX

Jung, W.-J.; Son, H.-J.; Pac, C.; Kang, S. O. Highly robust hybrid photocatalyst for carbon dioxide reduction: Tuning and optimization of catalytic activities of dye/TiO_2/Re(I) organic-inorganic ternary systems. *J. Am. Chem. Soc.* **2015**, *137*, 13679−13690.

(19) Windle, C. D.; Pastor, E.; Reynal, A.; Whitwood, A. C.; Vaynzof, Y.; Durrant, J. R.; Perutz, R. N.; Reisner, E. Improving the photocatalytic reduction of CO_2 to CO through immobilization of a molecular Re catalyst on TiO_2. *Chem. - Eur. J.* **2015**, *21*, 3746−3754.

(20) (a) Sahara, G.; Abe, R.; Higashi, M.; Morikawa, T.; Maeda, K.; Ueda, Y.; Ishitani, O. Photoelectrochemical CO_2 reduction using a Ru(II)-Re(I) multinuclear metal complex on a p-type semiconducting NiO electrode. *Chem. Commun.* **2015**, *51*, 10722−10725. (b) Sahara, G.; Kumagai, H.; Maeda, K.; Kaeffer, N.; Artero, V.; Higashi, M.; Abe, R.; Ishitani, O. Photoelectrochemical reduction of CO_2 coupled to water oxidation using a photocathode with a Ru(II)-Re(I) complex photocatalyst and a CoO_x/TaON photoanode. *J. Am. Chem. Soc.* **2016**, *138*, 14152−14158.

(21) Schreier, M.; Luo, J.; Gao, P.; Moehl, T.; Mayer, M. T.; Grätzel, M. Covalent immobilization of a molecular catalyst on Cu_2O photocathodes for CO_2 reduction. *J. Am. Chem. Soc.* **2016**, *138*, 1938−1946.

(22) Sullivan, B. P.; Bolinger, C. M.; Conrad, D.; Vining, W. J.; Meyer, T. J. One- and two-electron pathways in the electrocatalytic reduction of CO_2 by *fac*-Re(bpy)$(CO)_3$Cl (bpy = 2,2′-bipyridine). *J. Chem. Soc., Chem. Commun.* **1985**, 1414−1416.

(23) Paolucci, F.; Marcaccio, M.; Paradisi, C.; Roffia, S.; Bignozzi, C. A.; Amatore, C. Dynamics of the electrochemical behavior of diimine tricarbonyl rhenium(I) complexes in strictly aprotic media. *J. Phys. Chem. B* **1998**, *102*, 4759−4769.

(24) Hayashi, Y.; Kita, S.; Brunschwig, B. S.; Fujita, E. Involvement of a binuclear species with the Re-C(O)O-Re moiety in CO_2 reduction catalyzed by tricarbonyl rhenium(I) complexes with diimine ligands: Strikingly slow formation of the Re-Re and Re-C(O)O-Re species from Re(dmb)$(CO)_3$S (dmb = 4,4′-dimethyl-2,2′-bipyridine, S = solvent). *J. Am. Chem. Soc.* **2003**, *125*, 11976−11987.

(25) Fujita, E.; Muckerman, J. T. Why is Re-Re bond formation/cleavage in $[Re(bpy)(CO)_3]_2$ different from that in $[Re(CO)_5]_2$? Experimental and theoretical studies on the dimers and fragments. *Inorg. Chem.* **2004**, *43*, 7636−7647.

(26) Agarwal, J.; Fujita, E.; Schaefer, H. F., III; Muckerman, J. T. Mechanisms for CO production from CO_2 using reduced rhenium tricarbonyl catalysts. *J. Am. Chem. Soc.* **2012**, *134*, 5180−5186.

(27) Benson, E. E.; Kubiak, C. P. Structural investigations into the deactivation pathway of the CO_2 reduction electrocatalyst Re(bpy)-$(CO)_3$Cl. *Chem. Commun.* **2012**, *48*, 7374−7376.

(28) Liang, W.; Church, T. L.; Zheng, S.; Zhou, C.; Haynes, B. S.; D'Alessandro, D. M. Site isolation leads to stable photocatalytic reduction of CO_2 over a rhenium-based catalyst. *Chem. - Eur. J.* **2015**, *21*, 18576−18579.

(29) Machan, C. W.; Sampson, M. D.; Chabolla, S. A.; Dang, T.; Kubiak, C. P. Developing a mechanistic understanding of molecular electrocatalysts for CO_2 reduction using infrared spectroelectrochemistry. *Organometallics* **2014**, *33*, 4550−4559.

(30) Kou, Y.; Nabetani, Y.; Masui, D.; Shimada, T.; Takagi, S.; Tachibana, H.; Inoue, H. Direct detection of key reaction intermediates in photochemical CO_2 reduction sensitized by a rhenium bipyridine complex. *J. Am. Chem. Soc.* **2014**, *136*, 6021−6030.

(31) Grice, K. A.; Kubiak, C. P. Recent studies of rhenium and manganese bipyridine carbonyl catalysts for the electrochemical reduction of CO_2. *Adv. Inorg. Chem.* **2014**, *66*, 163−188.

(32) Bruckmeier, C.; Lehenmeier, M. W.; Reithmeier, R.; Rieger, B.; Herranz, J.; Kavakli, C. Binuclear rhenium(I) complexes for the photocatalytic reduction of CO_2. *Dalton Trans.* **2012**, *41*, 5026−5037.

(33) Tamaki, Y.; Imori, D.; Morimoto, T.; Koike, K.; Ishitani, O. High catalytic abilities of binuclear rhenium(I) complexes in the photochemical reduction of CO_2 with a ruthenium(II) photosensitizer. *Dalton Trans.* **2016**, *45*, 14668−14677.

(34) (a) Machan, C. W.; Chabolla, S. A.; Yin, J.; Gilson, M. K.; Tezcan, F. A.; Kubiak, C. P. Supramolecular assembly promotes the electrocatalytic reduction of carbon dioxide by Re(I) bipyridine catalysts at a lower overpotential. *J. Am. Chem. Soc.* **2014**, *136*, 14598−14607. (b) Machan, C. W.; Yin, J.; Chabolla, S. A.; Gilson, M. K.; Kubiak, C. P. Improving the efficiency and activity of electrocatalysts for the reduction of CO_2 through supramolecular assembly with amino acid-modified ligands. *J. Am. Chem. Soc.* **2016**, *138*, 8184−8193.

(35) (a) Shakeri, J.; Hadadzadeh, H.; Tavakol, H. Photocatalytic reduction of CO_2 to CO by a dinuclear carbonyl polypyridyl rhenium(I) complex. *Polyhedron* **2014**, *78*, 112−122. (b) Rezaei, B.; Mokhtarianpour, M.; Ensafi, A. A.; Hadadzadeh, H.; Shakeri, J. Electrocatalytic reduction of CO_2 using the dinuclear rhenium(I) complex $[ReCl(CO)_3(\mu\text{-tptzH})Re(CO)_3]$. *Polyhedron* **2015**, *101*, 160−164.

(36) (a) Wilting, A.; Stolper, T.; Mata, R. A.; Siewert, I. Dinuclear rhenium complex with a proton responsive ligand as a redox catalyst for the electrochemical CO_2 reduction. *Inorg. Chem.* **2017**, *56*, 4176−4185. (b) Wilting, A.; Siewert, I. A dinuclear rhenium complex with a proton responsive ligand in the electrochemical-driven CO_2-reduction catalysis. *ChemistrySelect* **2018**, *3*, 4593−4597.

(37) Guilard, R.; Lopez, M. A.; Tabard, A.; Richard, P.; Lecomte, C.; Brandes, S.; Hutchison, J. E.; Collman, J. P. Synthesis and characterization of novel cobalt aluminum cofacial porphyrins. First crystal and molecular structure of a heterobimetallic biphenylene pillared cofacial diporphyrin. *J. Am. Chem. Soc.* **1992**, *114*, 9877−9889.

(38) Wada, T.; Muckerman, J. T.; Fujita, E.; Tanaka, K. Substituents dependent capability of bis(Ru-dioxolene-tpy) complexes toward H_2O oxidation. *Dalton Trans.* **2011**, *40*, 2225−2233.

(39) The modest yield is due to incomplete separation of the two conformers, resulting in a subset of fractions that were not purified. The reported yield could be higher because these fractions were taken to dryness, accumulated with those of subsequent reactions, and later purified as described.

(40) Fraser, M. G.; Clark, C. A.; Horvath, R.; Lind, S. J.; Blackman, A. G.; Sun, X.-Z.; George, M. W.; Gordon, K. C. Complete family of mono-, bi-, and trinuclear $Re^{I}(CO)_3Cl$ complexes of the bridging polypyridyl ligand 2,3,8,9,14,15-hexamethyl-5,6,11,12,17,18-hexaazatrinaphthalene: *Syn/anti* isomer separation, characterization, and photophysics. *Inorg. Chem.* **2011**, *50*, 6093−6106.

(41) (a) Randles, J. E. B. A cathode ray polarograph. Part II.-The current-voltage curves. *Trans. Faraday Soc.* **1948**, *44*, 327−338. (b) Bard, A. J.; Faulkner, L. R. *Electrochemical Methods: Fundamentals and Applications*, 2nd ed.; John Wiley and Sons: New York, 2001.

(42) Richardson, D. E.; Taube, H. Mixed-valence molecules: Electronic delocalization and stabilization. *Coord. Chem. Rev.* **1984**, *60*, 107−129.

(43) Manes, T. A.; Rose, M. J. Redox properties of a bis-pyridine rhenium carbonyl derived from an anthracene scaffold. *Inorg. Chem. Commun.* **2015**, *61*, 221−224.

(44) Savéant, J. M.; Vianello, E. Potential-sweep chronoamperometry theory of kinetic currents in the case of a first order chemical reaction preceding the electron-transfer process. *Electrochim. Acta* **1963**, *8*, 905−923.

(45) Nicholson, R. S.; Shain, I. Theory of stationary electrode polarography. Single scan and cyclic methods applied to reversible, irreversible, and kinetic systems. *Anal. Chem.* **1964**, *36*, 706−723.

(46) Rountree, E. S.; McCarthy, B. D.; Eisenhart, T. T.; Dempsey, J. L. Evaluation of homogeneous electrocatalysts by cyclic voltammetry. *Inorg. Chem.* **2014**, *53*, 9983−10002.

(47) Huang, D.; Makhlynets, O. V.; Tan, L. L.; Lee, S. C.; Rybak-Akimova, E. V.; Holm, R. H. Kinetics and mechanistic analysis of an extremely rapid carbon dioxide fixation reaction. *Proc. Natl. Acad. Sci. U. S. A.* **2011**, *108*, 1222−1227.

(48) (a) Steffey, B. D.; Curtis, C. J.; DuBois, D. L. Electrochemical reduction of CO_2 catalyzed by a dinuclear palladium complex containing a bridging hexaphosphine ligand: Evidence for coopera-

DOI: 10.1021/acs.inorgchem.8b01775
Inorg. Chem. XXXX, XXX, XXX−XXX

tivity. *Organometallics* **1995**, *14*, 4937−4943. (b) Raebiger, J. W.; Turner, J. W.; Noll, B. C.; Curtis, C. J.; Miedaner, A.; Cox, B.; DuBois, D. L. Electrochemical reduction of CO_2 to CO catalyzed by a bimetallic palladium complex. *Organometallics* **2006**, *25*, 3345−3351.

(49) Liu, S.; Senocak, A.; Smeltz, J. L.; Yang, L.; Wegenhart, B.; Yi, J.; Kenttämaa, H. I.; Ison, E. A.; Abu-Omar, M. M. Mechanism of MTO-catalyzed deoxydehydration of diols to alkenes using sacrificial alcohols. *Organometallics* **2013**, *32*, 3210−3219.

(50) Soler-Yanes, R.; Arribas-Álvarez, I.; Guisán-Ceinos, M.; Buñuel, E.; Cárdenas, D. J. NiI catalyzes the regioselective cross-coupling of alkylzinc halides and propargyl bromides to allenes. *Chem. - Eur. J.* **2017**, *23*, 1584−1590.

(51) Ngo, K. T.; McKinnon, M.; Mahanti, B.; Narayanan, R.; Grills, D. C.; Ertem, M. Z.; Rochford, J. Turning on the protonation-first pathway for electrocatalytic CO_2 reduction by manganese bipyridyl tricarbonyl complexes. *J. Am. Chem. Soc.* **2017**, *139*, 2604−2618.

(52) (a) Costentin, C.; Drouet, S.; Robert, M.; Savéant, J.-M. Turnover numbers, turnover frequencies, and overpotential in molecular catalysis of electrochemical reactions. Cyclic voltammetry and preparative-scale electrolysis. *J. Am. Chem. Soc.* **2012**, *134*, 11235−11242. (b) Costentin, C.; Robert, M.; Savéant, J.-M.; Costentin, C.; Robert, M.; Savéant, J.-M. Catalysis of the electrochemical reduction of carbon dioxide. *Chem. Soc. Rev.* **2013**, *42*, 2423−2436.

(53) Wiedner, E. S.; Bullock, R. M. Electrochemical detection of transient cobalt hydride intermediates of electrocatalytic hydrogen production. *J. Am. Chem. Soc.* **2016**, *138*, 8309−8313.

(54) No significant differences were observed in the estimated TOFs from FOWA when using E^0_{cat} rather than $E_{cat/2}$ in eq 3, except the TOF versus scan rate plots (Figure S16) were more well-behaved before reaching the scan-rate-independent TOF maximum when using $E_{cat/2}$. Because of the slow catalysis following the initial overlapping one-electron reductions of the dinuclear catalysts, the linear portion of the FOWA plots was used to estimate the TOFs.

(55) Wong, K.-Y.; Chung, W.-H.; Lau, C.-P. The effect of weak Brönsted acids on the electrocatalytic reduction of carbon dioxide by a rhenium tricarbonyl bipyridyl complex. *J. Electroanal. Chem.* **1998**, *453*, 161−170.

(56) Smieja, J. M.; Benson, E. E.; Kumar, B.; Grice, K. A.; Seu, C. S.; Miller, A. J. M.; Mayer, J. M.; Kubiak, C. P. Kinetic and structural studies, origins of selectivity, and interfacial charge transfer in the artificial photosynthesis of CO. *Proc. Natl. Acad. Sci. U. S. A.* **2012**, *109*, 15646−15650.

(57) It has been shown that the pK_a values of weak acids are very similar between DMSO and DMF. Maran, F.; Celadon, D.; Severin, M. G.; Vianello, E. Electrochemical determination of the pK_a of weak acids in *N,N*-dimethylformamide. *J. Am. Chem. Soc.* **1991**, *113*, 9320−9329.

(58) Olmstead, W. N.; Margolin, Z.; Bordwell, F. G. Acidities of water and simple alcohols in dimethyl sulfoxide solution. *J. Org. Chem.* **1980**, *45*, 3295−3299.

(59) Taft, R. W.; Bordwell, F. G. Structural and solvent effects evaluated from acidities measured in dimethyl sulfoxide and in the gas phase. *Acc. Chem. Res.* **1988**, *21*, 463−469.

(60) Bordwell, F. G.; McCallum, R. J.; Olmstead, W. N. Acidities and hydrogen bonding of phenols in dimethyl sulfoxide. *J. Org. Chem.* **1984**, *49*, 1424−1427.

(61) Pegis, M. L.; Roberts, J. A. S.; Wasylenko, D. J.; Mader, E. A.; Appel, A. M.; Mayer, J. M. Standard reduction potentials for oxygen and carbon dioxide couples in acetonitrile and *N,N*-dimethylformamide. *Inorg. Chem.* **2015**, *54*, 11883−11888.

(62) Appel, A. M.; Helm, M. L. Determining the overpotential for a molecular electrocatalyst. *ACS Catal.* **2014**, *4*, 630−633.

(63) Lee, G. R.; Maher, J. M.; Cooper, N. J. Reductive disproportionation of carbon dioxide by dianionic carbonylmetalates of the transition metals. *J. Am. Chem. Soc.* **1987**, *109*, 2956−2962.

(64) Ratliff, K. S.; Lentz, R. E.; Kubiak, C. P. Carbon dioxide chemistry of the trinuclear complex $[Ni_3(\mu_3\text{-CNMe})(\mu_3\text{-I})(dppm)_3][PF_6]$. Electrocatalytic reduction of carbon dioxide. *Organometallics* **1992**, *11*, 1986−1988.

(65) Fei, H.; Sampson, M. D.; Lee, Y.; Kubiak, C. P.; Cohen, S. M. Photocatalytic CO_2 reduction to formate using a Mn(I) molecular catalyst in a robust metal-organic framework. *Inorg. Chem.* **2015**, *54*, 6821−6828.

(66) (a) Bolinger, C. M.; Sullivan, B. P.; Conrad, D.; Gilbert, J. A.; Story, N.; Meyer, T. J. Electrocatalytic reduction of CO_2 based on polypyridyl complexes of rhodium and ruthenium. *J. Chem. Soc., Chem. Commun.* **1985**, 796−797. (b) Bolinger, C. M.; Story, N.; Sullivan, B. P.; Meyer, T. J. *Inorg. Chem.* **1988**, *27*, 4582−4587.

(67) Sampson, M. D.; Froehlich, J. D.; Smieja, J. M.; Benson, E. E.; Sharp, I. D.; Kubiak, C. P. Direct observation of the reduction of carbon dioxide by rhenium bipyridine catalysts. *Energy Environ. Sci.* **2013**, *6*, 3748−3755.

(68) Christensen, P. A.; Hamnett, A.; Muir, A. V. G.; Freeman, N. A. CO_2 reduction at platinum, gold, and glassy carbon electrodes in acetonitrile. An in-situ FTIR study. *J. Electroanal. Chem. Interfacial Electrochem.* **1990**, *288*, 197−215.

(69) Cheng, S. C.; Blaine, C. A.; Hill, M. G.; Mann, K. R. Electrochemical and IR spectroelectrochemical studies of the electrocatalytic reduction of carbon dioxide by $[Ir_2(dimen)_4]^{2+}$ (dimen = 1,8-diisocyanomenthane). *Inorg. Chem.* **1996**, *35*, 7704−7708.

(70) Takeda, H.; Koike, K.; Inoue, H.; Ishitani, O. Development of an efficient photocatalytic system for CO_2 reduction using rhenium(I) complexes based on mechanistic studies. *J. Am. Chem. Soc.* **2008**, *130*, 2023−2031.

(71) *APEX2*, version 2009.1; Bruker Analytical X-ray Systems Inc.: Madison, WI, 2009.

(72) Sheldrick, G. M. *SADABS*, version 2.03; Bruker Analytical X-ray Systems Inc.: Madison, WI, 2000.

(73) (a) Sheldrick, G. M. Phase annealing in SHELX-90: Direct methods for larger structures. *Acta Crystallogr., Sect. A: Found. Crystallogr.* **1990**, *46*, 467−473. (b) Sheldrick, G. M. A short history of SHELX. *Acta Crystallogr., Sect. A: Found. Crystallogr.* **2008**, *64*, 112−122. (c) Sheldrick, G. M. *SHELXL-2014/7: Program for crystal structure determination*; University of Göttingen: Göttingen, Germany, 2014.

(74) (a) Spek, A. L. *PLATON: A Multipurpose Crystallographic Tool*; Utrecht University: Utrecht, The Netherlands, 2007. (b) Spek, A. L. PLATON SQUEEZE: A tool for the calculation of the disordered solvent contribution to the calculated structure factors. *Acta Crystallogr., Sect. C: Struct. Chem.* **2015**, *71*, 9−18.

(75) Frisch, M. J.; et al. *Gaussian 09*, revision D.01; Gaussian, Inc.: Wallingford, CT, 2009.

(76) Lin, Y.-S.; Li, G.-D.; Mao, S.-P.; Chai, J.-D. Long-range corrected hybrid density functionals with improved dispersion corrections. *J. Chem. Theory Comput.* **2013**, *9*, 263−272.

(77) Minenkov, Y.; Singstad, Å.; Occhipinti, G.; Jensen, V. R. The accuracy of DFT-optimized geometries of functional transition metal compounds: A validation study of catalysts for olefin metathesis and other reactions in the homogeneous phase. *Dalton Trans.* **2012**, *41*, 5526−5541.

(78) Caspar, J. V.; Meyer, T. J. Application of the energy gap law to nonradiative, excited-state decay. *J. Phys. Chem.* **1983**, *87*, 952−957.

(79) Böttger, M.; Wiegmann, B.; Schaumburg, S.; Jones, P. G.; Kowalsky, W.; Johannes, H.-H. Synthesis of new pyrrole-pyridine-based ligands using an in situ Suzuki coupling method. *Beilstein J. Org. Chem.* **2012**, *8*, 1037−1047.

DOI: 10.1021/acs.inorgchem.8b01775
Inorg. Chem. XXXX, XXX, XXX−XXX